Available online at www.sciencedirect.com
SCIENCE DIRECT®
International Journal of Solids and Structures 42 (2005) 2755–2770
INTERNATIONAL JOURNAL OF SOLIDS and STRUCTURES
www.elsevier.com/locate/ijsolstr

A new method to study dilatant deformation mechanisms in ductile materials

Aleksander Zubelewicz *

Los Alamos National Laboratory, MST-8, MS G755, Los Alamos, NM 87545, USA

Received 22 April 2004; received in revised form 28 September 2004
Available online 5 November 2004

Abstract

This paper presents an unconventional method for examining various kinematically admissible and physically acceptable mechanisms of dilatant deformation in ductile materials. In this approach, the constitutive description of material behavior is intentionally left incomplete, i.e., shear stresses and strain rates obey power law, but while material dilatancy is allowed to exist, its form is not predetermined. By omitting the constitutive equation for dilatancy, multiple boundary value solutions can be obtained; these solutions can be further examined and evaluated using an energy minimization criterion. The proposed method allows plausible constitutive assumptions for cavitation to be identified. Using this method, we show that in the vicinity of a mode I crack tip, there are three distinct mechanisms of dilatant deformation, each having strong experimental justification.
Published by Elsevier Ltd.

Keywords: Dilatancy; Cavitation; Ductility; Mode I crack; HRR distribution

1. Introduction

Typically, solving a boundary value problem requires that constitutive equations and boundary conditions be completely identified. Our difficulties begin when some of the constitutive responses are not well understood and, then, suppose that dilatancy in ductile materials is such a property in question. This paper describes a suitable method for studying such an incompletely defined problem. In this analysis, the constitutive equation for dilatancy is intentionally omitted. As a consequence, there are not one but several boundary value solutions for which dilatant deformation obeys kinematical compatibility, stresses satisfy equilibrium conditions, and boundary conditions are properly determined. An additional energy based

* Tel.: +1 505 665 1498; fax: +1 505 667 8021.
E-mail address: alek@lanl.gov

0020-7683/$ - see front matter Published by Elsevier Ltd.
doi:10.1016/j.ijsolstr.2004.09.044

Nomenclature

$(x,y),(R,\theta),(z,z^*)$ coordinate systems
ψ,ψ^*,Ω stress functions
$\sigma_{\text{eq}},I_\sigma,\sigma_{ij}$ Tresca (maximum shear) stress, hydrostatic stress, and stress components
τ,τ^*,η,η^* complex conjugate shear stresses and strains
$e_{\text{eq}},I_\varepsilon,\varepsilon_{ij}$ equivalent (maximum shear) strain, volumetric strain, and strain components
u_x,u_y,v,v^* (x,y) and complex conjugate displacements
M_{ij},N_{ij},q,α microstructural tensors and microstructural parameters
W^d,W^s,W^c energy dissipation in the surroundings of a crack tip
Λ,σ_0,p material constants
λ stress singularity factor
$C,C^*,D_i,D_i^*,\alpha_n,\beta_n,\delta_n,H_i^n,H_i^{nm},H_i^{nmk}$ constants

criterion and certain restrictions must be introduced to further select a desired solution. Here, we select valid deformation mechanisms by minimizing the dissipation energy. In addition, rate of the energy dissipation due to dilatancy and the dilatancy itself are nonnegative quantities at each point of a ductile material. Based on the derivations presented here, we show that cavities may nucleate in ductile materials when a certain pattern of an inelastic deformation is present. More precisely, when the requirement of kinematical compatibility is imposed and the energy dissipation is kept at the minimum level, a ductile material may be forced to exhibit dilatational deformation. When cavitation does not occur or when it is directly coupled with stresses, such a solution to the boundary value problem becomes unique, that is, only one state of stresses and deformation can be determined.

The proposed approach offers an opportunity to study various kinematically admissible mechanisms of dilatant deformation. We show that for the mode I crack problem, there is not one but three mechanisms of cavitation, each of them associated with a unique pattern of stresses. Furthermore, our theoretical predictions suggest that the rate of the dissipation energy density might not obey the 1/R singularity in the cavitating surroundings of a crack tip. Departure from the $1/R$ HRR (Hutchinson, Rice, and Rosengren) distribution makes sense (Rice, 2001) when the constitutive equation for cavitation is not described in terms of potentials. It is worth mentioning that Guduru et al. (2001) presented experimental data that seem to support the departure from the $1/R$ distribution.

2. Microstructural nature of inelastic flow

The homogenization technique employed in this analysis is based on the known concept introduced by Hill (1972) and further explored by Hill and Rice (1972) that the bilinear stress and strain form is invariant under changes of measure or reference state. Using this concept, Zubelewicz (1990, 1993) showed that the internal structure of a crystalline material can be modeled by a set of representative discontinuity planes imperfectly embedded into an elastic matrix; both the planes and the matrix occupy a characteristic volume ΔV. Local slippages along these planes and crystal (grain) rotations cause macroscopically observed deformation. As shown, the homogenized plastic dilatant strain rates can be defined as follows:

$$\dot{\varepsilon}_{ij} = M_{ij}\dot{e}_{\text{eq}}, \tag{2.1}$$

where $\dot{e}_{eq}$ is the equivalent strain rate and M_{ij} represents the microstructural tensor

$$M_{ij} = \frac{1}{2}(N_{ij} + qN_{ik}N_{kj}). \tag{2.2}$$

The tensors $N_{ij} = (n_i s_j + s_i n_j)$ and $N_{ik}N_{kj} = (n_i n_j + s_i s_j)$ satisfy the following conditions:

$$N_{ij} = N_{ij}^{2n+1}, \quad N_{ij}^2 = N_{ij}^{2n}, \quad N_{kk} = 0, \quad N_{kk}^2 = 2, \tag{2.3}$$

in which $n = 1, 2, 3, \ldots, \infty$. The orthogonal vectors, n_i and s_j, describe an average (homogenized) normal and slip direction in the deformed material. The function q indicates the material's readiness for cavitation. In this notation, the microstructural tensors are $N_{ij}^2 = N_{ik}N_{kj}$, $N_{ij}^3 = N_{ik}N_{kl}N_{lj}$ and so on. When slip is restricted to a single plane (plane stress or plane strain), there are only three components of the tensor M_{ij}:

$$\begin{aligned} M_{xx} &= \frac{1}{2}(\cos\alpha + q), \\ M_{yy} &= \frac{1}{2}(-\cos\alpha + q), \\ M_{xy} &= \frac{1}{2}\sin\alpha, \end{aligned} \tag{2.4}$$

where the functions α and q may vary within the material, $\alpha = \alpha(x, y)$ and $q = q(x, y)$. A general three-dimensional expression of the tensor was presented in Zubelewicz (1993). The strain rates $\dot{\varepsilon}_{xx}, \dot{\varepsilon}_{yy}$, and $\dot{\varepsilon}_{xy}$ are obtained by substituting (2.4) into (2.1). Subsequently, the strain rates are rewritten as

$$\begin{aligned} \Delta\dot{\varepsilon} &= \dot{\varepsilon}_{xx} - \dot{\varepsilon}_{yy} = \dot{e}_{eq}\cos\alpha, \\ \dot{\varepsilon}_{xy} &= \frac{1}{2}\dot{e}_{eq}\sin\alpha, \\ \dot{I}_{\varepsilon} &= \dot{\varepsilon}_{xx} + \dot{\varepsilon}_{yy} = q\dot{e}_{eq}, \end{aligned} \tag{2.5}$$

and brought into the following form:

$$\begin{aligned} \dot{\eta} &= \Delta\dot{\varepsilon} + 2i\dot{\varepsilon}_{xy} = e^{i\alpha}\dot{e}_{eq}, \\ \dot{\eta}^* &= \Delta\dot{\varepsilon} - 2i\dot{\varepsilon}_{xy} = e^{-i\alpha}\dot{e}_{eq}, \\ \dot{I}_{\varepsilon} &= q\dot{e}_{eq}, \end{aligned} \tag{2.6}$$

where $i = \sqrt{-1}$. The complex conjugate shear strain rates ($\dot{\eta}$ and $\dot{\eta}^*$) are defined through the function α and the equivalent strain rate $\dot{e}_{eq}$, while q is the strain rate triaxiality ratio, $q = \dot{I}_{\varepsilon}/\dot{e}_{eq}$. In the analysis to follow, the strain rate triaxiality ratio does not need to be specified. The complex strain rates and stresses are expressed through the (z, z^*) complex variables, where $z = x + iy$ and $z^* = x - iy$.

3. Displacements

The complex shear strains η and η^* are coupled with complex displacements as shown:

$$\begin{aligned} \eta &= 2\frac{\partial v}{\partial z^*}, \\ \eta^* &= 2\frac{\partial v^*}{\partial z}, \end{aligned} \tag{3.1}$$

where $v = u_x + iu_y$, $v^* = u_x - iu_y$, while u_x and u_y denote displacements in x and y directions. Now, the displacements u_x and u_y can be expressed through the complex shear strains η and η^* as follows:

$$u_x = \frac{1}{4}\left[\int \eta\,\mathrm{d}z^* + \int \eta^*\,\mathrm{d}z\right] + \frac{1}{2}\left[\psi_v(z) + \psi_v^*(z^*)\right],$$
$$u_y = \frac{1}{4\mathrm{i}}\left[\int \eta\,\mathrm{d}z^* - \int \eta^*\,\mathrm{d}z\right] + \frac{1}{2\mathrm{i}}\left[\psi_v(z) - \psi_v^*(z^*)\right]. \tag{3.2}$$

The additional displacement functions ψ_v and ψ_v^* help in maintaining nonnegative values of the energy dissipation and dilatancy. It must be noted that η and η^* are nonanalytic complex conjugate functions, thus the product of integration (Eq. (3.2)) is path dependent. This problem is resolved by choosing a path-dependent integration, where one of the complex variables is kept constant while integrating with respect to the other variable (Vakula, 1962). Knowing that $\dot{I}_\varepsilon = \partial\dot{u}_x/\partial x + \partial\dot{u}_y/\partial y$, the volumetric strain rate is calculated directly from (3.2),

$$\dot{I}_\varepsilon = \frac{1}{2}\int \frac{\partial\dot{\eta}}{\partial z}\,\mathrm{d}z^* + \frac{1}{2}\int \frac{\partial\dot{\eta}^*}{\partial z^*}\,\mathrm{d}z + \dot{\psi}_v'(z) + \dot{\psi}_v^{*\prime}(z^*), \tag{3.3}$$

where $\psi_v' = \partial\psi_v/\partial z$.

4. Kinematical compatibility

For plane strain, the kinematical compatibility equation

$$\frac{\partial^2\dot{\varepsilon}_{xx}}{\partial y^2} + \frac{\partial^2\dot{\varepsilon}_{yy}}{\partial x^2} = 2\frac{\partial^2\dot{\varepsilon}_{xy}}{\partial x\,\partial y} \tag{4.1}$$

is rewritten using the complex variables (z, z^*), where the strain rates ($\dot{\varepsilon}_{xx}$, $\dot{\varepsilon}_{yy}$, and $\dot{\varepsilon}_{xy}$) are replaced by the complex shear strain rates ($\dot{\eta}$, $\dot{\eta}^*$) and the volumetric strain rate $\dot{I}_\varepsilon$. Derivations not replicated in this paper lead to the following result:

$$\frac{\partial^2\dot{\eta}}{\partial z^2} + \frac{\partial^2\dot{\eta}^*}{\partial (z^*)^2} = 2\frac{\partial^2\dot{I}_\varepsilon}{\partial z\,\partial z^*}. \tag{4.2}$$

The rate of cavitation $\dot{I}_\varepsilon$ described by (3.3) satisfies the kinematical requirement (4.2).

5. Flow rules

An assumption that the inelastic deformation is triggered by the current stress σ_{kl} implies that the components of the microstructural tensor M_{ij} must be coupled with the stress components σ_{kl}, therefore $M_{ij} = M_{ij}(\sigma_{kl})$. As mentioned earlier, a general three-dimensional relationship that satisfies the conditions in (2.3) is presented in Zubelewicz (1993). When slip occurs at a single plane, the tensor components are equal to

$$M_{xx} = \frac{1}{2}\left(\frac{\Delta\sigma}{\sqrt{\Delta\sigma^2 + 4\sigma_{xy}^2}} + q\right),$$
$$M_{yy} = \frac{1}{2}\left(\frac{-\Delta\sigma}{\sqrt{\Delta\sigma^2 + 4\sigma_{xy}^2}} + q\right), \tag{5.1}$$
$$M_{xy} = \frac{\sigma_{xy}}{\sqrt{\Delta\sigma^2 + 4\sigma_{xy}^2}},$$

where the stress $\Delta\sigma$ is equal to $\Delta\sigma = \sigma_{xx} - \sigma_{yy}$. It is convenient to replace $(\sigma_{xx}, \sigma_{yy}, \sigma_{xy})$ with complex stresses defined as follows:

$$\begin{aligned} \tau &= \Delta\sigma + 2\mathrm{i}\sigma_{xy}, \\ \tau^* &= \Delta\sigma - 2\mathrm{i}\sigma_{xy}, \\ I_\sigma &= \sigma_{xx} + \sigma_{yy}. \end{aligned} \tag{5.2}$$

Then, the ratio of the complex shear strain rates $\dot{\eta}/\dot{\eta}^*$, expressed as

$$\frac{\dot{\eta}}{\dot{\eta}^*} = \frac{\Delta\dot{\varepsilon} + 2\mathrm{i}\dot{\varepsilon}_{xy}}{\Delta\dot{\varepsilon} - 2\mathrm{i}\dot{\varepsilon}_{xy}} = \frac{(M_{xx} - M_{yy} + 2\mathrm{i}M_{xy})\dot{e}_{\mathrm{eq}}}{(M_{xx} - M_{yy} - 2\mathrm{i}M_{xy})\dot{e}_{\mathrm{eq}}} = \frac{\Delta\sigma + 2\mathrm{i}\sigma_{xy}}{\Delta\sigma - 2\mathrm{i}\sigma_{xy}} = \frac{\tau}{\tau^*} = e^{2\mathrm{i}\alpha}, \tag{5.3}$$

is equal to the ratio of the complex shear stresses τ/τ^*, and is a function of the angle α alone, where $\alpha = \arctan(2\sigma_{xy}/\Delta\sigma)$. In this analysis, the stress component σ_{zz} is irrelevant because the deformation defined by (2.1) and (2.2) is restricted to a single plane.

6. Power-law constitutive relations

In this analysis, the equivalent stress σ_{eq} is defined as

$$\sigma_{\mathrm{eq}} = \frac{1}{2} N_{ij}\sigma_{ij} = \frac{1}{2}\sqrt{\tau\tau^*}. \tag{6.1}$$

The equivalent stress σ_{eq} is in fact the Tresca stress (the maximum shear stress). The equivalent strain rate (maximum shear strain rate) is derived directly from (2.6) and is equal to

$$\dot{e}_{\mathrm{eq}} = \sqrt{\dot{\eta}\dot{\eta}^*}. \tag{6.2}$$

The power-law constitutive equation

$$\dot{e}_{\mathrm{eq}} = \Lambda\left(\frac{\sigma_{\mathrm{eq}}}{\sigma_0}\right)^p \tag{6.3}$$

couples the equivalent strain rate $\dot{e}_{\mathrm{eq}}$ and stress σ_{eq}. The stress exponent p identifies the desired deformation mechanism, Λ is a material constant, and σ_0 is a material strength. The relations (5.3)–(6.3) allow construction of two constitutive equations:

$$\begin{aligned} \dot{\eta} &= \frac{\Lambda}{(2\sigma_0)^p}\tau^{p+1/2}(\tau^*)^{p-1/2}, \\ \dot{\eta}^* &= \frac{\Lambda}{(2\sigma_0)^p}(\tau^*)^{p+1/2}\tau^{p-1/2}, \end{aligned} \tag{6.4}$$

which couple the complex shear strain rates with complex shear stresses. Note that neither the in-plane pressure I_σ nor the rate of cavitation $\dot{I}_\varepsilon$ enters the relations (6.4). Thus, there is a convenient decoupling between the material responses due to shear and dilatancy. The constitutive equations become linear when p is equal to one. When p approaches infinity, $p \to \infty$, this model describes a rigid plastic behavior. Then, the equivalent stress σ_{eq} is constant and the complex stresses are expressed through the angle α and the yield stress σ_0,

$$\begin{aligned} \sigma_{\mathrm{eq}} &= \frac{1}{2}\sqrt{\tau\tau^*} = \sigma_0, \\ \tau &= 2\sigma_0 e^{\mathrm{i}\alpha}, \\ \tau^* &= 2\sigma_0 e^{-\mathrm{i}\alpha}. \end{aligned} \tag{6.5}$$

The first equation in (6.5) represents the known Tresca criterion.

7. Equilibrium equations

The equilibrium equations are re-derived for a plane problem. We replace the stress components $(\sigma_{xx}, \sigma_{yy}, \sigma_{xy})$ with the complex stresses(τ, τ^*, I_σ), and then rather simple derivations lead to the following result:

$$\begin{aligned} &\frac{\partial \tau}{\partial z} + \frac{\partial I_\sigma}{\partial z^*} = 0, \\ &\frac{\partial \tau^*}{\partial z^*} + \frac{\partial I_\sigma}{\partial z} = 0. \end{aligned} \tag{7.1}$$

It is worth mentioning that Wu and Hui (1987) used this form of the equilibrium equations to solve an elastic crack problem. In our approach, we satisfy the equations with the use of two stress functions $\psi_\sigma(z)$ and $\Omega(z, z^*)$ chosen as

$$\begin{aligned} \tau &= \psi_\sigma^*(z^*) + \int \frac{\partial \Omega}{\partial z^*}\, \mathrm{d}z, \\ \tau^* &= \psi_\sigma(z) + \int \frac{\partial \Omega}{\partial z}\, \mathrm{d}z^*, \\ I_\sigma &= -\Omega, \end{aligned} \tag{7.2}$$

where Ω is a real function defined through the complex variables z and z^*. In these equations, we integrate the function Ω with respect to either z or z^*, while the other variable is constant.

8. Criterion of minimum energy

At this point of the analysis, there are five governing equations: two equilibrium equations (7.1), two constitutive equations (6.4), and the kinematical compatibility equation (3.3) or (4.2). On the other hand, we need to determine three complex stresses (τ, τ^*, and I_σ) and three strain rate components ($\dot{\eta}$, $\dot{\eta}^*$, and $\dot{I}_\varepsilon$), thus six functions. Note that some of the functions are coupled. Therefore there are three independent governing equations and four functions to be determined. As a consequence, several solutions may satisfy the requirements of the statical and kinematical admissibility. Selection of an additional constitutive equation for dilatancy $\dot{I}_\varepsilon$ or an assumption of the material's incompressibility restores the uniqueness of the solutions.

In this analysis, however, the sixth equation that describes the volumetric change in the material is deliberately omitted. This treatment provides the opportunity to study various kinematically admissible mechanisms of dilatant deformation. Among all available solutions only some are considered for further analysis. Further screening is based on the assumption that the desired deformation mechanism has some physical significance. Based on the arguments by Prigogine (1977), when internal and external boundary conditions prevent a system from reaching thermodynamic equilibrium (that is, zero entropy production), the system settles down to the state of "least dissipation." In our system, the dissipative mechanism consists of slippage and dilatancy. While slippage is well described, the dilatancy is allowed to take any form that is both kinematically admissible and physically acceptable. This requires that the dissipation energy in the ΔV surrounding the crack tip be at the minimum level. It will be shown that size of the volume ΔV is irrelevant. From (2.1) and (6.1), the rate of energy dissipation is equal to

$$\dot{W}^t = \frac{1}{2}\int_{\Delta V} \sigma_{ij}\left(N_{ij} + qN_{ik}N_{kj}\right)\dot{e}_{\mathrm{eq}}\, \mathrm{d}V = \int_{\Delta V} \sigma_{\mathrm{eq}}\dot{e}_{\mathrm{eq}}\, \mathrm{d}V + \frac{1}{2}\int_{\Delta V} I_\sigma \dot{I}_\varepsilon\, \mathrm{d}V. \tag{8.1}$$

Here, $\dot{W}^s = \int_{\Delta V} \sigma_{\text{eq}} \dot{e}_{\text{eq}} \, \mathrm{d}V$ is the energy rate due to slip and $\dot{W}^c = \frac{1}{2} \int_{\Delta V} I_\sigma \dot{I}_\varepsilon \, \mathrm{d}V$ results from nucleation and growth of voids. In this approach, the energy rate due to slip is always equal to or greater than zero. Additional requirements are put in place to assure that both the energy rate due to cavitation, $\frac{1}{2} I_\sigma \dot{I}_\varepsilon$, and the cavitation itself have nonnegative values at each point in the deformed material.

9. Near crack tip solutions

The stress functions ψ_σ and Ω discussed earlier are defined as

$$\begin{aligned} \psi_\sigma &= \sum_n C_n z^{\lambda_n}, \\ \Omega &= \sum_{n,m} \left[D_{nm} z^{\alpha_m^n} (z^*)^{\beta_m^n} + D^*_{nm} z^{\beta_m^n} (z^*)^{\alpha_m^n} \right], \end{aligned} \tag{9.1}$$

where the stress exponent λ_n is required to satisfy the condition $\lambda_n = \alpha_m^n + \beta_m^n$ for any n and m defined between one and infinity. The stress coefficients C_n, C^*_n, D_{nm}, and D^*_{nm} reflect boundary conditions of the problem under consideration. In case of an asymptotic analysis, the index n can be dropped and the complex stresses defined by (7.2) become

$$\begin{aligned} \tau &= C^* (z^*)^\lambda + \sum_m \left[\frac{\beta_m D_m}{\alpha_m + 1} z^{\alpha_m + 1} (z^*)^{\beta_m - 1} + \frac{\alpha_m D^*_m}{\beta_m + 1} z^{\beta_m + 1} (z^*)^{\alpha_m - 1} \right], \\ \tau^* &= C z^\lambda + \sum_m \left[\frac{\beta_m D^*_m}{\alpha_m + 1} (z^*)^{\alpha_m + 1} z^{\beta_m - 1} + \frac{\alpha_m D_m}{\beta_m + 1} (z^*)^{\beta_m + 1} z^{\alpha_m - 1} \right], \\ I_\sigma &= -\sum_m \left[D_m z^{\alpha_m} (z^*)^{\beta_m} + D^*_m z^{\beta_m} (z^*)^{\alpha_m} \right]. \end{aligned} \tag{9.2}$$

It is already assured that the complex stresses satisfy the equilibrium conditions (7.1). The amplitude of the stress functions (9.2) is given by the stress coefficients C and C^*, while the ratios D_m/C, D^*_m/C, D_m/C^*, D^*_m/C^* are the non-dimensional complex constants.

10. Boundary conditions

The boundary conditions for free crack surfaces are written as

$$\sigma_{yy} + \mathrm{i}\sigma_{xy} = 0 \tag{10.1}$$

for $\theta = \pm\pi$, where θ is the angle in the polar coordinate system (R, θ) shown in Fig. 1. The boundary conditions are further rewritten using the complex stresses, and Eq. (10.1) becomes

$$\sigma_{yy} + \mathrm{i}\sigma_{xy} = \frac{1}{2}(I_\sigma - \tau^*) = 0, \quad \text{for } \theta = \pm\pi. \tag{10.2}$$

In the polar coordinate system, where $z = R(\cos\theta + \mathrm{i}\sin\theta)$ and $z^* = R(\cos\theta - \mathrm{i}\sin\theta)$, the above condition leads to four equations:

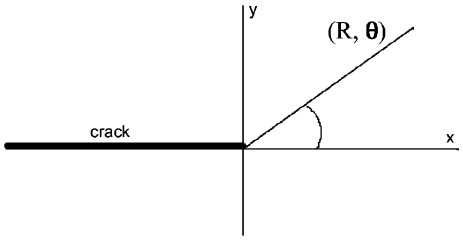

Fig. 1. Polar coordinate system attached to the crack tip.

$$
\begin{aligned}
&C^1\cos\lambda\pi+\sum_m\frac{(\lambda+1)(\lambda+2)}{(\alpha_m+1)(\beta_m+1)}D_m^1\cos(\alpha_m-\beta_m)\pi=0,\\
&C^1\sin\lambda\pi+\sum_m\frac{(\lambda+1)(\alpha_m-\beta_m)}{(\alpha_m+1)(\beta_m+1)}D_m^1\sin(\alpha_m-\beta_m)\pi=0,\\
&C^2\cos\lambda\pi+\sum_m\frac{(\lambda+1)(\alpha_m-\beta_m)}{(\alpha_m+1)(\beta_m+1)}D_m^2\cos(\alpha_m-\beta_m)\pi=0,\\
&C^2\cos\lambda\pi+\sum_m\frac{(\lambda+1)(\lambda+2)}{(\alpha_m+1)(\beta_m+1)}D_m^2\sin(\alpha_m-\beta_m)\pi=0,
\end{aligned}
\tag{10.3}
$$

in which $m=1,2,\ldots,\infty$, $C=C^1+\mathrm{i}C^2$, and $D=D^1+\mathrm{i}D^2$. In particular, when $C^2=0$ and $D_m^2=0$, these equations describe the boundary conditions for the mode I crack problem. Here, the parameters α_m and β_m can be calculated from

$$
\begin{aligned}
&(\lambda+2)\tan[(\lambda+2)\pi]=(\alpha_m-\beta_m)\tan[(\alpha_m-\beta_m)\pi],\\
&\lambda=\alpha_m+\beta_m,
\end{aligned}
\tag{10.4}
$$

where $m=1,2,\ldots,\infty$. For each λ, there is an infinite number of pairs α_m and β_m, (see Fig. 2).

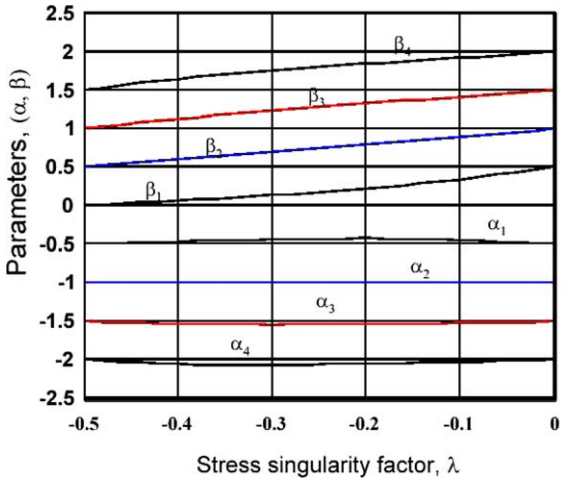

Fig. 2. Pairs α_n and β_n for varying stress singularity factor λ.

11. Mode I crack problem for $p = 3$

In the analysis to follow, the ductile material is assumed to obey the power-law constitutive equation (6.3), where the stress exponent is assumed to be equal to 3. Furthermore, the stress components (τ, τ^*, and I_σ) and strain rates ($\dot{\eta}$, $\dot{\eta}^*$, and $\dot{I}_\varepsilon$) are expressed in terms of the polar coordinate system (R, θ). As a consequence, the equivalent stress σ_{eq}, in-plane pressure I_σ, equivalent strain rate $\dot{e}_{\text{eq}}$, and dilatancy $\dot{I}_\varepsilon$, are all defined through the variables R and θ. The equivalent stress σ_{eq} is derived from (6.1) and takes the following form:

$$\sigma_{\text{eq}} = \frac{1}{2} R^\lambda \tilde{\sigma}_{\text{eq}}(\theta), \tag{11.1}$$

where

$$\begin{aligned}\tilde{\sigma}^2_{\text{eq}}(\theta) = {} & (C^1)^2 + 2C^1 \sum_n D^1_n \rho^\beta_n \cos(\lambda + \delta_n + 2)\theta + 2C^1 \sum_n D^1_n \rho^\alpha_n \cos(\lambda - \delta_n + 2)\theta \\ & + 2 \sum_{n,m} D^1_n D^1_m \rho^\alpha_n \rho^\beta_m \cos(\delta_n + \delta_m)\theta + \sum_{n,m} D^1_n D^1_m \left(\rho^\alpha_n \rho^\beta_m + \rho^\beta_n \rho^\alpha_m \right) \cos(\delta_n - \delta_m)\theta.\end{aligned} \tag{11.2}$$

The factors ρ^α_n and ρ^β_n are defined as $\rho^\alpha_n = \alpha_n/(\beta_n + 1)$, $\rho^\beta_n = \beta_n/(\alpha_n + 1)$. Since the parameter α_2 is constant and equal to minus one, $\alpha_2 = -1$, the factors ρ^β_2 are singular for all stress exponents λ. In the analysis to follow, the second term in the stress functions Ω is omitted. The parameter C^1 is the amplitude of the stress function (9.2) and the ratios (D^1_n/C^1) are non-dimensional factors. The parameters δ_n are equal to $\delta_n = \alpha_n - \beta_n$. Taking into account all the above, the in-plane pressure defined through (9.2) is equal to

$$I_\sigma = -2R^\lambda \sum_n D^1_n \cos \delta_n \theta. \tag{11.3}$$

The complex shear strain rates are calculated from (6.4) and (3.3). For $p = 3$, the equation for cavitation

$$\dot{I}_\varepsilon = \frac{\Lambda}{8\sigma^3_0} \left[\int \frac{\partial(\tau^2 \tau^*)}{\partial z} \, \mathrm{d}z^* + \int \frac{\partial \left[(\tau^*)^2 \tau \right]}{\partial z^*} \, \mathrm{d}z \right] + \left(\dot{\psi}'_v + \dot{\psi}^{*\prime}_v \right) \tag{11.4}$$

becomes

$$\dot{I}_\varepsilon = \frac{\Lambda R^{3\lambda}}{4\sigma^3_0} \dot{\tilde{I}}_\varepsilon(\theta), \tag{11.5}$$

where

$$\begin{aligned}\dot{\tilde{I}}_\varepsilon(\theta) = {} & A^1 \cos 3\lambda\theta + \frac{\lambda (C^1)^3}{2\lambda + 1} \cos(\lambda + 2)\theta + 2(C^1)^2 \sum_n D^1_n H^n_2 \cos \delta_n \theta + (C^1)^2 \sum_n D^1_n H^n_3 \cos(2\lambda + \delta_n + 4)\theta + (C^1)^2 \\ & \times \sum_n D^1_n H^n_4 \cos(2\lambda - \delta_n + 4)\theta + C^1 \sum_{n,m} D^1_n D^1_m H^{nm}_5 \cos(\lambda + \delta_n + \delta_m + 2)\theta \\ & + C^1 \sum_{n,m} D^1_n D^1_m H^{nm}_6 \cos(\lambda + \delta_n - \delta_m + 2)\theta + C^1 \sum_{n,m} D^1_n D^1_m H^{nm}_7 \cos(\lambda - \delta_n + \delta_m + 2)\theta \\ & + C^1 \sum_{n,m} D^1_n D^1_m H^{nm}_8 \cos(\lambda - \delta_n - \delta_m + 2)\theta + \sum_{n,m,k} D^1_n D^1_m D^1_k H^{nmk}_9 \cos(\delta_n + \delta_m + \delta_k)\theta \\ & + \sum_{n,m,k} D^1_n D^1_m D^1_k H^{nmk}_{10} \cos(\delta_n - \delta_m + \delta_k)\theta + \sum_{n,m,k} D^1_n D^1_m D^1_k H^{nmk}_{11} \cos(\delta_n - \delta_m - \delta_k)\theta \\ & + \sum_{n,m,k} D^1_n D^1_m D^1_k H^{nmk}_{12} \cos(\delta_n + \delta_m - \delta_k)\theta.\end{aligned} \tag{11.6}$$

The term $(A^1\cos 3\lambda\theta)$ in the above expression comes from the function $(\dot{\psi}_v' + \dot{\psi}_v^{*'})$ in (3.3), where A^1 is a constant. The function $(\dot{\psi}_v' + \dot{\psi}_v^{*'})$ has singularity of the same order as the other strain functions. Also, $(\dot{\psi}_v' + \dot{\psi}_v^{*'})$ must satisfy the symmetry condition for $(\pm\theta)$. The constants (A^1 and D_n^1) will be determined by bringing the dissipation energy to minimum. All the other parameters in (11.6) are equal to

$$
\begin{aligned}
H_2^n &= \frac{\rho_n^\beta(\lambda+\alpha_n+1)}{\lambda+\beta_n} + \frac{\rho_n^\alpha(\lambda+\beta_n+1)}{\lambda+\alpha_n},\\
H_3^n &= \frac{\rho_n^\beta(\beta_n-1)}{2\lambda+\alpha_n+2},\\
H_4^n &= \frac{\rho_n^\alpha(\alpha_n-1)}{2\lambda+\beta_n+2},\\
H_5^{nm} &= \frac{\rho_n^\beta\rho_m^\beta(\lambda+\alpha_n+\alpha_m+2)}{\beta_n+\beta_m-1} + 2\frac{\rho_n^\alpha\rho_m^\beta(\beta_n+\beta_m)}{\lambda+\alpha_n+\alpha_m+1},\\
H_6^{nm} &= \frac{\rho_n^\beta\rho_m^\alpha(\lambda+\alpha_n+\beta_m+2)}{\beta_n+\alpha_m-1} + 2\frac{\rho_n^\alpha\rho_m^\alpha(\beta_n+\alpha_m)}{\lambda+\alpha_n+\beta_m+1},\\
H_7^{nm} &= \frac{\rho_n^\alpha\rho_m^\beta(\lambda+\beta_n+\alpha_m+2)}{\alpha_n+\beta_m-1} + 2\frac{\rho_n^\beta\rho_m^\beta(\alpha_n+\beta_m)}{\lambda+\beta_n+\alpha_m+1},\\
H_8^{nm} &= \frac{\rho_n^\alpha\rho_m^\alpha(\lambda+\beta_n+\beta_m+2)}{\alpha_n+\alpha_m-1} + 2\frac{\rho_n^\beta\rho_m^\alpha(\alpha_n+\alpha_m)}{\lambda+\beta_n+\beta_m+1},\\
H_9^{nmk} &= \frac{\rho_n^\beta\rho_m^\beta\rho_k^\alpha(\alpha_n+\alpha_m+\alpha_k+1)}{\beta_n+\beta_m+\beta_k} + \frac{\rho_n^\alpha\rho_m^\alpha\rho_k^\beta(\beta_n+\beta_m+\beta_k+1)}{\alpha_n+\alpha_m+\alpha_k},\\
H_{10}^{nmk} &= \frac{\rho_n^\beta\rho_m^\alpha\rho_k^\alpha(\alpha_n+\beta_m+\alpha_k+1)}{\beta_n+\alpha_m+\beta_k} + \frac{\rho_n^\alpha\rho_m^\beta\rho_k^\beta(\beta_n+\alpha_m+\beta_k+1)}{\alpha_n+\beta_m+\alpha_k},\\
H_{11}^{nmk} &= \frac{\rho_n^\beta\rho_m^\alpha\rho_k^\beta(\alpha_n+\beta_m+\beta_k+1)}{\beta_n+\alpha_m+\alpha_k} + \frac{\rho_n^\alpha\rho_m^\beta\rho_k^\alpha(\beta_n+\alpha_m+\alpha_k+1)}{\alpha_n+\beta_m+\beta_k},\\
H_{12}^{nmk} &= \frac{\rho_n^\beta\rho_m^\beta\rho_k^\beta(\alpha_n+\alpha_m+\beta_k+1)}{\beta_n+\beta_m+\alpha_k} + \frac{\rho_n^\alpha\rho_m^\alpha\rho_k^\alpha(\beta_n+\beta_m+\alpha_k+1)}{\alpha_n+\alpha_m+\beta_k}.
\end{aligned}
\tag{11.7}
$$

12. Mechanisms of dilatant deformation

The mode I crack solutions are developed for the stress function Ω assumed in the form of a four- and six-term series, where the second term is omitted. It is found that the two stress functions produce similar results. For comparison, contours of the equivalent stress $\sigma_{eq}/\sigma_0 = 1$ for an incompressible material ($\lambda = -0.25$) are shown in Fig. 5a. It is a special case, where the expressions (11.1) and (11.2) approximate well the HRR stress field, while the dilatancy (11.6) reduces to zero. Since the analysis is computationally intensive, a decision was made to continue this study using the four-term stress function. As assumed, the material's dilatancy $\dot{I}_\varepsilon$ is permitted as long as it helps in restoring the kinematical compatibility, while rate of the energy dissipation due to dilatancy is nonnegative. Under this condition, there is more than one solution available for further analysis. Final selection of the deformation mechanisms is based on the requirement that the dissipation energy in ΔV is at a minimum level. For the asymptotic crack problem, it is convenient to write the criterion in a form of the energy ratio $\dot{W}^c/\dot{W}^s$, in which all solutions are scaled such that rate of the energy dissipation due to shear $\dot{W}^s$ is equal to $\dot{W}^s = 1R^{4\lambda}$. Because singularity of both the energies (due to slip and cavitation) is same, the size of the volume ΔV becomes irrelevant. The energy is

calculated in the crack surroundings$\Delta V = R_0^2\pi$, where R_0 can be selected arbitrarily and, therefore, is assumed to be one. The energy is minimized with respect to the parameters A^1 and D_n^1 ($n = 1,3,4$). A numerical minimization procedure was developed, in which each solution is obtained for a predetermined value of the stress exponent λ. It is assured that the rate of dissipation due to cavitation $\dot{W}^c$ and the dilatancy $\dot{I}_\varepsilon$ are non-negative quantities for all values of the angle θ checked with a precision of 1° within the domain $(0, 2\pi)$. We find that there is more than one such minimum for the mode I crack problem. In course of the analysis, three independent mechanisms of dilatant deformation were identified and plotted as a function of the stress singularity factorλ (Figs. 3 and 4). As shown in Figs. 5–8, each mechanism has a characteristic distribution of stresses (σ_{RR}, $\sigma_{R\theta}$, and $\sigma_{\theta\theta}$), the equivalent stress $\sigma_{\text{eq}}/\sigma_0 = 1$, and the rate of cavitation $\dot{I}_\varepsilon/\Lambda = const$. It is worth mentioning that the contours of the equivalent stress (Tresca stress), defined here by the radius R_σ and plotted as a function of θ,

$$R_\sigma = \left[\frac{\tilde{\sigma}_{\text{eq}}(\theta)}{2\sigma_0}\right]^{-1/\lambda}, \tag{12.1}$$

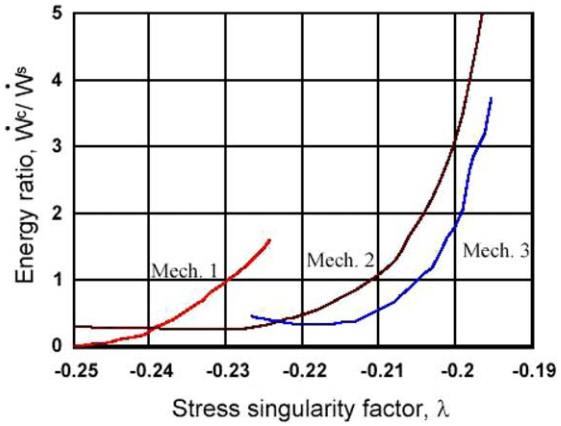

Fig. 3. Plots of energy ratio versus stress singularity factor.

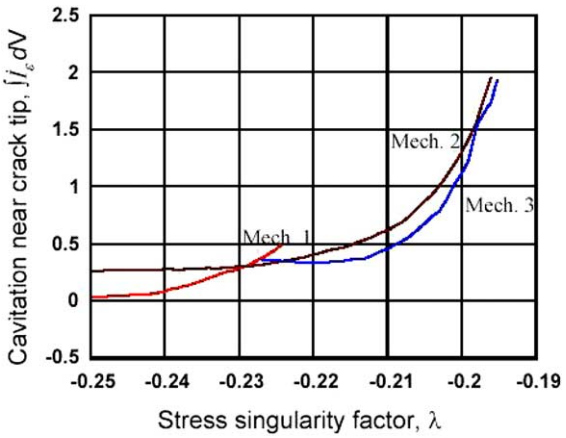

Fig. 4. Cavitation in the crack tip surroundings versus stress singularity factor.

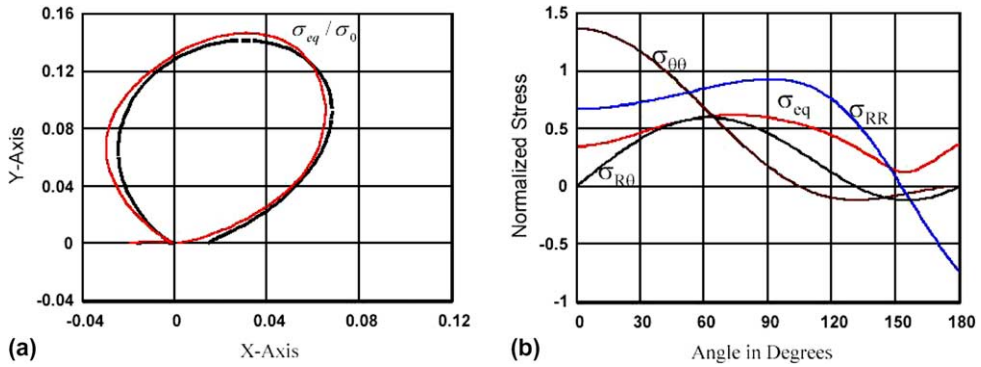

Fig. 5. (a) Contours of the maximum shear stress, mechanism 1, $\lambda = -0.25$. Broken line corresponds to a 4-term stress function, the solid line to a 6-term stress function. (b) Normalized stresses as a function of angle θ mechanism 1, $\lambda = -0.25$. Approximation: 4-term stress function.

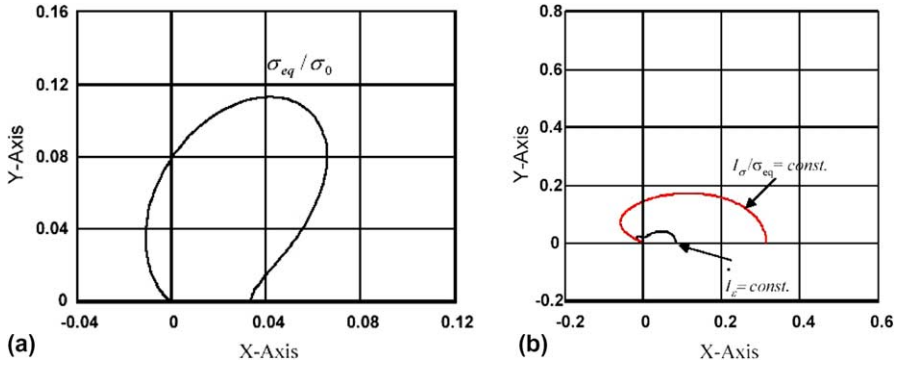

Fig. 6. (a) Contour of constant equivalent stress, mechanism 1, $\lambda = -0.23$. (b) Contours of constant cavitation and stress triaxiality ratio, mechanism 1, $\lambda = -0.23$.

are identical to the contours of the equivalent strain rate, $\dot{e}_{\mathrm{eq}}/\Lambda = \mathrm{const}$. The constant rate of cavitation $\dot{I}_\varepsilon/\Lambda = \mathrm{const}$ is calculated and plotted in a similar manner.

12.1. Mechanism 1 cavitation controlled by the stress triaxiality ratio (I_σ/σ_{eq})

Mechanism 1 is characterized using 44 values of the stress singularity factor λ in the range of -0.250 to -0.226. The first solution is found for λ equal to -0.250. This is the only case where the deformation is free of dilatancy. Plots of the stresses ($\sigma_{RR}, \sigma_{R\theta}$, and $\sigma_{\theta\theta}$) shown in Fig. 5a and b are similar to the ones obtained by Rice and Rosengren (1968) as well as Hutchinson (1968). All the other solutions within the mechanism are associated with a dilatant deformation. This mechanism expires for $\lambda = -0.226$. This analysis suggests that the dilatancy is controlled by the stress triaxiality ratio, $\dot{I}_\varepsilon = \dot{I}_\varepsilon(I_\sigma/\sigma_{\mathrm{eq}})$. As shown in Fig. 6b, contours of the constant rate of cavitation $\dot{I}_\varepsilon$ and the stress triaxiality ratio $I_\sigma/\sigma_{\mathrm{eq}}$ have similar shape for the whole range of the stress singularity factor λ. When the cavitation rate becomes more pronounced, the shape of the stress contour σ_{eq} evolves, (compare Figs. 5a and 6a). It is worth noting that our stress contours resemble the contours obtained numerically by Needleman and Tvergaard (1991). In the latter case, the material is assumed to obey the flow potential, introduced by Gurson (1977), in which the void growth is controlled

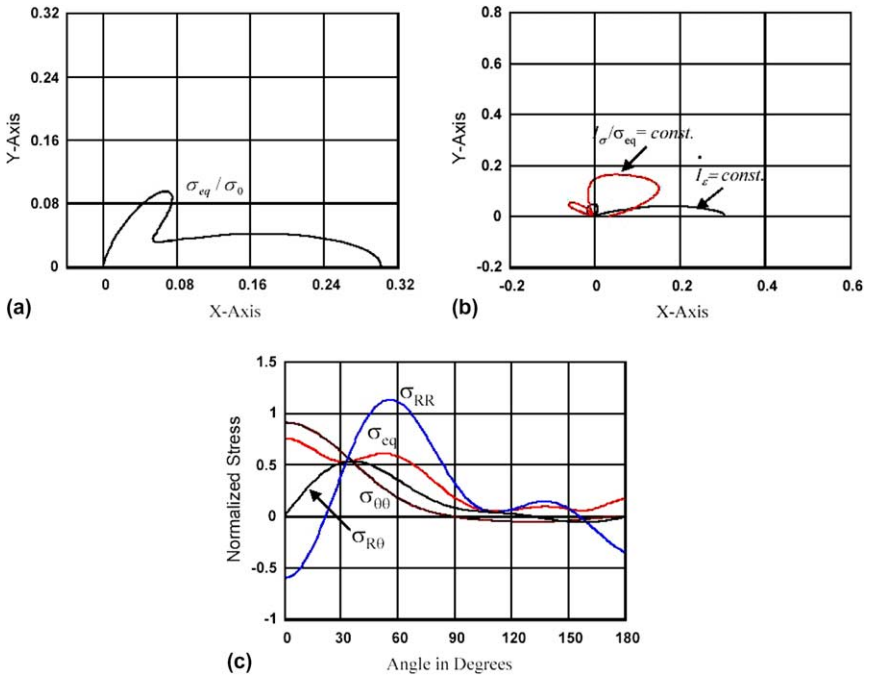

Fig. 7. (a) Contour of constant equivalent stress, mechanism 2, $\lambda = -0.23$. (b) Contours of constant cavitation and stress triaxiality ratio, mechanism 2, $\lambda = -0.23$. (c) Normalized stresses as a function of angle θ mechanism 2, $\lambda = -0.23$.

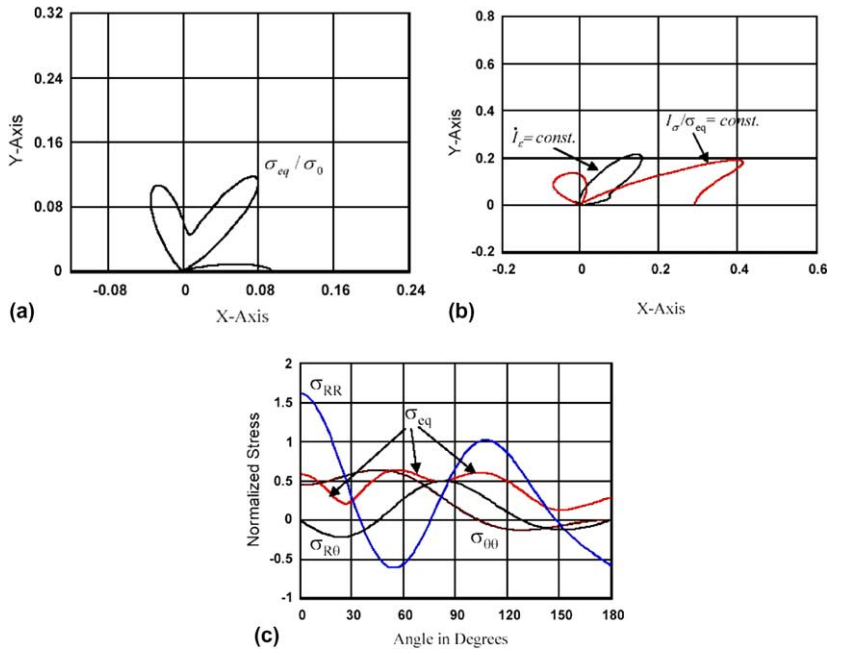

Fig. 8. (a) Contour of constant equivalent stress, mechanism 3, $\lambda = -0.225$. (b) Contours of constant cavitation and stress triaxiality ratio, mechanism 3, $\lambda = -0.225$. (c) Normalized stresses as a function of angle θ mechanism 2, $\lambda = -0.225$.

by the stress triaxiality ratio, while void nucleation is described in terms of the shear stress and pressure, matrix strain rate, and stress rates. Furthermore, Onck and van der Giessen (1999) developed a model in which the matetrial that surrounds the crack tip is represented discreetly by grains and grain boundaries, while the far field material is described as a continuum. As shown, a small-scale cavitation modifies the HRR stress distribution only slightly. We observe the same trends in our analysis, as shown in Figs. 5a and 6a. We predict that this mechanism expires when minimum of the energy is no longer distinguishable from the numerical noise. For λ greater than 0.226, a small perturbation applied to the parameters A^1 or D_n^1 ($n = 1,3,4$) brings the energy ratio to another minimum—a minimum that is associated with mechanism 2.

12.2. Mechanism 2 cavitation governed by the equivalent stress σ_{eq}

This mechanism is found for 55 values of λ taken from the range -0.250 to -0.196. Mechanism 2 describes the deformation that is localized within a narrow process zone extending straight ahead of the crack tip, Fig. 7a. Peak values of the maximum tensile stress ($\sigma_{\theta\theta}$) are found to be directly ahead of the crack tip, Fig. 7c. Behind the crack tip, all the stress components are nearly equal to zero. In this case, there is no correlation between the stress triaxiality ratio and dilatancy, Fig. 7b. Instead, the rate of cavitation seems to be proportional to the maximum tensile stress and/or the equivalent shear stress.

12.3. Mechanism 3 unknown stress dependence

The third mechanism is investigated by selecting 35 values of λ within the range -0.227 to -0.195. In this case, the maximum shear strain rate is localized within three narrow zones, as shown in Fig. 8a. This response can be explained by the observed waviness in the equivalent stress σ_{eq} when plotted against the angle θ, Fig. 8c. The mechanism generates much greater values of the energy dissipation due to dilatancy when compared with the ones in the mechanism 1. The analysis shows that a significant dilatancy develops in the direction of about 55° with respect to the crack plane. The dilatational zone coincides with one of the three shear branches, Fig. 8b. Onck and van der Giessen (1999) predicted a similar mechanism for a ductile material that is in an advanced stage of dilatational fracture. Extensive grain boundary rotation (the second term in Eq. (2.2)) can be blamed for the unique pattern of stresses and deformation. Yet, the dilatancy itself has an unspecified stress origin. It cannot be linked with either the stress triaxiality ratio or the maximum tensile stress. Further analysis must follow to better understand and physically validate the mechanism.

12.4. Coexistence of deformation mechanisms

The theoretical analysis indicates that there is more than one mechanism by which cavities nucleate and grow ahead of a mode I crack tip. The dilatational damage begins under the deformation process described by mechanism 1. This mechanism expires and is either replaced by mechanism 2 or it may bifurcate and become mechanism 3. Multiple mechanisms are known to coexist near a mode I crack tip. Hayherst et al. (1984) reported that different patterns of crack growth exist in an aluminum alloy (D19S), copper, and 316 stainless steel. Ozmat et al. (1991) observed branching of a crack in stainless steel (Type 304) at high temperature (600–775 °C) in plane strain. In their case, a pre-fatigued sharp crack propagates on a plane at an angle of 50° with the median plane of the initial crack. Mechanism 3 describes this growth well. Since the crack propagated in a pre-cracked, fatigued material, it is likely that mechanism 1 expired and was replaced by mechanism 3. In another experiment conducted by Ozmat et al., a specimen with no pre-crack fatigue having a blunt notch of a finite radius was subjected to constant loading. In this case, the crack propagated along the median plane, as predicted by both the mechanisms 1 and 2. Later, the crack bifurcated and propagated at about 50°; it then changed path again to become parallel to the median plane. In

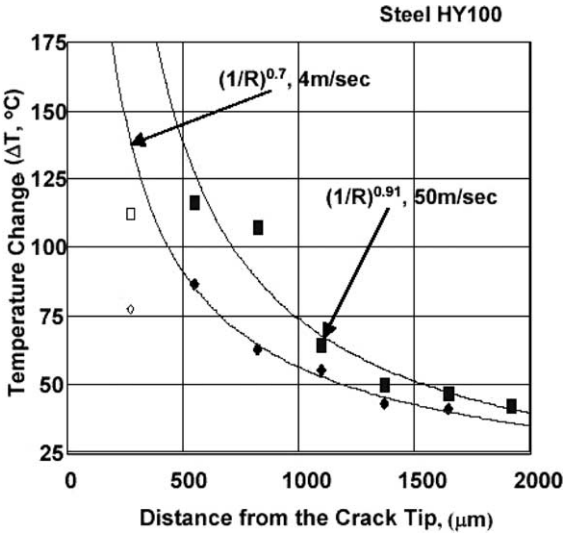

Fig. 9. Deviation of energy density rate from $1/R$ HRR field (reproduced data from Guduru et al., 2001).

addition, Guduru et al. (2001) have observed all the cavitation mechanisms under dynamic load conditions in high strength C300 maraging steel and in ductile HY100 steel.

12.5. Departure from the 1/R HRR distribution

The present analysis suggests that the stress and strain singularity near the cavitating crack tip may not obey the $1/R$ HRR singularity, as suggested by Rice and Rosengren (1968) as well as Hutchinson (1968). One plausible explanation is that the available energy is converted not only to the surface energy of a propagating crack but also is consumed by voids growing in the region surrounding the crack. Experimental data presented by Guduru et al. (2001) indicates that the energy density rate $\sigma_{ij}\dot{e}_{ij}$ near the cavitating crack tip, measured as a function of temperature change under nearly adiabatic conditions, may indeed deviate from the commonly accepted $1/R$ HRR type of distribution. This deviation was magnified by an increased rate of cavitation, Fig. 9. We find that the data by Guduru et al. for a very high velocity impact (50 m/s) plotted as a function of the temperature distribution around a mode I crack tip followed a power-law relationship ($1/R^{0.91}$) and that a significant change in the response occurred upon a slower impact (4 m/s), still well within the range of adiabatic conditions, where a ($1/R^{0.7}$) temperature distribution best fit the data. Our present analysis agrees with these experimental results and indicates that the deviation from a $1/R$ distribution is expected, however, it is a self-limiting phenomenon. Mechanism 1 expires when the singularity of the energy density is equal to $(1/R)^{0.89}$. Mechanisms 2 and 3 expire for λ in the range of -0.196 to -0.195, corresponding to an energy singularity on the order of $(1/R)^{0.78}$.

13. Conclusions

Typically, the phenomenon of void nucleation is linked with stresses. While there is no doubt that stresses magnify the process of cavity nucleation and growth, one may also agree with Alvez and Jones (1999) that a material's dilatancy is a reflection of a strain pattern in the material. Since an inelastic shear

deformation alone might not satisfy the requirement of kinematical compatibility, we speculate that the cavitation described by Eq. (3.3) may be required to restore the compatibility.

The proposed analytical approach is useful in solving the mode I crack problem. One interesting feature of this method is that various kinematically admissible mechanisms of cavitation, which may develop near a stress singularity point, can be explored. Although the true nature of cavitation processes is still open and needs further investigation, our analysis suggests probable deformation mechanisms that may occur in a cavitating material. It seems that the cavitation process is first coupled with the stress triaxiality ratio. An initial sharp crack produces very high stresses, therefore this mechanism is expected to expire quickly and becomes either the Daugdale–Barrenblatt mechanism, or bifurcate and be replaced by the mechanism that is associated with large plastic deformation localized within three shear bands. Our analysis shows that not one but two or even three constitutive responses are possible during the deformation process. Most certainly, further study must be conducted to properly address the issue.

We are in the process of extending this method to study various kinematically admissible and physically acceptable modes of deformation in complex structures, including, various forms of dilatational deformation in metals subjected to extreme (shock) conditions.

References

Alvez, M., Jones, N., 1999. Influence of hydrostatic stress on failure of axisymmetric notched specimen. J. Mech. Phys. Solids 47, 643–667.

Guduru, P.R., Zehner, A.T., Rosakis, A.J., Ravichandran, G., 2001. Dynamic full field measurements of crack tip temperatures. Eng. Fract. Mech. 38, 371–402.

Gurson, A.L., 1977. Continuum theory of ductile rapture by void nucleation and growth. 1. Yield criteria and flow rules for porous ductile media. J. Engng. Mater. Technol. 99, 2–15.

Hill, R., 1972. On Constitutive macro-variables for heterogeneous solids at finite strains. Proc. Roy. Soc. Lond. Ser. A 326, 131–147.

Hill, R., Rice, J.R., 1972. Constitutive analysis of elasto-plastic crystals at arbitrary strains. J. Mech. Phys. Solids 20, 401–413.

Hutchinson, J.W., 1968. Singular behaviour at the end of a tensile crack in a hardening material. J. Mech. Phys. Solids 16, 13–31.

Hayherst, D.R., Brown, P.R., Morrison, C.J., 1984. The role of continuum damage in creep crack growth. Philos. Trans. Roy. Soc. Lond. A311, 131–158.

Needleman, A., Tvergaard, V., 1991. An analysis of dynamic, ductile crack growth in a double edge cracked specimen. Int. J. Fract. 49, 41–67.

Prigogine, I., 1977. Time, Structure, and Fluctuations. Nobel Lecture, Nobel Price in Chemistry, Royal Academy of Sweden.

Onck, P.R., van der Giessen, E., 1999. Growth of an initially sharp crack by grain boundary cavitation. J. Mech. Phys. Solids 47, 99–139.

Ozmat, B., Argon, A.S., Parks, D.M., 1991. Growth modes of cracks in creeping type 304 stainless steel. Mech. Mater. 11, 1–17.

Rice, J.R., Rosengren, G.F., 1968. Plane strain deformation near a crack tip in a power-law hardening material. J. Mech. Phys. Solids 16, 1–12.

Rice, J.R., 2001. Private communications.

Vakula, N., 1962. Generalized analytic functions. Series of Monographs in Pure and Applied Mathematics, 25. Pergamon Press, Inc., pp. 23–27.

Wu, K.C., Hui, C.Y., 1987. A Complex variable method for two dimensional internal stress problems and its application to crack growth in non-elastic materials (Parts 1 and 2). J. Appl. Mech., Trans. ASME 54, 59–71.

Zubelewicz, A., 1990. Overall stress and strain rates for crystalline and frictional materials. Int. J. Non-Linear Mech. 25, 389–393.

Zubelewicz, A., 1993. Micromechanical study of ductile polycrystalline materials. J. Mech. Phys. Solids 41, 1711–1722.